

Contents lists available at ScienceDirect

#### Acta Biomaterialia

journal homepage: www.elsevier.com/locate/actabiomat



Full length article

## Thermosensitive, fast gelling, photoluminescent, highly flexible, and degradable hydrogels for stem cell delivery



Hong Niu<sup>a</sup>, Xiaofei Li<sup>a</sup>, Haichang Li<sup>b</sup>, Zhaobo Fan<sup>a</sup>, Jianjie Ma<sup>b</sup>, Jianjun Guan<sup>a,c,\*</sup>

- <sup>a</sup> Department of Materials Science and Engineering, The Ohio State University, 2041 College Road, Columbus, OH, USA
- <sup>b</sup> Department of Surgery, The Ohio State University, Columbus, OH 43210, USA
- <sup>c</sup> Department of Mechanical Engineering and Materials Science, Washington University in St. Louis, St. Louis, MO 63130, USA

#### ARTICLE INFO

# Article history: Received 18 May 2018 Received in revised form 23 October 2018 Accepted 23 October 2018 Available online 26 October 2018

Keywords:
Fast gelling hydrogels
Photoluminescent hydrogels
Cell retention
Real-time cell tracking
Stem cell therapy

#### ABSTRACT

Stem cell therapy is a promising approach to regenerate ischemic cardiovascular tissues yet experiences low efficacy. One of the major causes is inferior cell retention in tissues. Injectable cell carriers that can quickly solidify upon injection into tissues so as to immediately increase viscosity have potential to largely improve cell retention. A family of injectable, fast gelling, and thermosensitive hydrogels were developed for delivering stem cells into heart and skeletal muscle tissues. The hydrogels were also photoluminescent with low photobleaching, allowing for non-invasively tracking hydrogel biodistribution and retention by fluorescent imaging. The hydrogels were polymerized by N-isopropylacrylamide (NIPAAm), 2-hydroxyethyl methacrylate (HEMA), 1-vinyl-2-pyrrolidinone (VP), and acrylateoligolactide (AOLA), followed by conjugation with hypericin (HYP). The hydrogel solutions had thermal transition temperatures around room temperature, and were readily injectable at 4 °C. The solutions were able to quickly solidify within 7 s at 37 °C. The formed gels were highly flexible possessing similar moduli as the heart and skeletal muscle tissues. In vitro, hydrogel fluorescence intensity decreased proportionally to weight loss. After being injected into thigh muscles, the hydrogel can be detected by an in vivo imaging system for 4 weeks. The hydrogels showed excellent biocompatibility in vitro and in vivo, and can stimulate mesenchymal stem cell (MSC) proliferation and paracrine effects. The fast gelling hydrogel remarkably increased MSC retention in thigh muscles compared to slow gelling collagen, and non-gelling PBS. These hydrogels have potential to efficiently deliver stem cells into tissues. Hydrogel degradation can be non-invasively and real-time tracked.

#### **Statement of Significance**

Low cell retention in tissues represents one of the major causes for limited therapeutic efficacy in stem cell therapy. A family of injectable, fast gelling, and thermosensitive hydrogels that can quickly solidify upon injection into tissues were developed to improve cell retention. The hydrogels were also photoluminescent, allowing for non-invasively and real-time tracking hydrogel biodistribution and retention by fluorescent imaging.

© 2018 Acta Materialia Inc. Published by Elsevier Ltd. All rights reserved.

#### 1. Introduction

Ischemic cardiovascular diseases such as myocardial infarction (MI) and critical limb ischemia (CLI) affect millions of people in the world [1,2]. The ischemic cardiac tissue and limbs are characterized by extensive cell death, poor blood perfusion, and ischemic

E-mail address: jguan22@wustl.edu (J. Guan).

environment. Restoration of blood perfusion to relieve ischemia, and promotion of cardiac muscle and skeletal muscle regeneration are key therapeutic goals for MI and CLI [3–8]. Stem cell therapy represents a promising approach to achieve these goals [3–11]. Various animal studies have demonstrated that stem cell therapy could, to some extent, improve blood perfusion in the ischemic hearts and limbs, and even stimulate muscle repair in these tissues [3–11]. However, clinical trials have shown only a transient therapeutic benefit [3–12]. In general, current stem cell therapy exhibits a relatively low efficacy. One of the key causes is inferior cell retention in ischemic tissues [3,5,12,13]. A common approach used to

<sup>\*</sup> Corresponding author at: Department of Mechanical Engineering and Materials Science, Washington University in St. Louis, Campus Box 1185, One Brookings Drive, St. Louis, MO 63130, USA.

deliver stem cells is to suspend cells in saline followed by injection. While this minimally invasive approach is attractive for clinical application, a large percentage of injected saline/cells is leaked out during and after the injection [3,5,12,13]. Several studies have demonstrated that only  $\sim$ 20% of cells remained in the ischemic limbs 24 h after transplantation [13–16]. This is mainly attributed to the low viscosity of saline solution [3,5,12,13]. The intact and elastic muscle tissues can readily squeeze the saline and stem cells out. To increase cell retention, higher viscosity polymeric injectable hydrogels may be used as cell carriers as they can be more easily immobilized in the tissues. Different hydrogels have been employed for stem cell delivery into infarcted hearts and limbs, such as fibrin [17-19], alginate [20-23], collagen [24,25], Matrigel [26], hyaluronic acid [27,28], chitosan [29], decellularized extracellular matrix [30-32], and PEG-PCL-PEG [33]. While these hydrogels have been shown to increase cell retention for an extent. the efficiency remains low due to their relatively slow gelation rate. These hydrogels cannot quickly increase viscosity upon injection so as to be efficiently retained in the tissues. Therefore, fast gelling hydrogels are critical for largely increasing cell retention [21].

Efficacy of the stem cell therapy is also determined by the distribution of cells and hydrogels in the ischemic tissues, and number of cells engrafted with the host tissues [3-12]. Uniform distribution of stem cells and hydrogels may facilitate tissue regeneration [3-12]. To monitor stem cell and hydrogel distribution, non-invasive fluorescence imaging is clinically appealing as it is more convenient than other non-invasive imaging techniques such as magnetic resonance imaging and X-ray computed tomography that require complicated instruments [34]. In addition, radiopaque contrast agents are required for magnetic resonance imaging and X-ray computed tomography. These agents may not be able to readily penetrate into the hydrogels if they are injected into body before imaging. They may gradually release from the hydrogels if the agents are encapsulated in the hydrogels, thus not allowing for real-time monitoring for extended period. Following fluorescence imaging, cell and hydrogel distribution can be quickly informed. Imaging of stem cells may be achieved by using cells that are pre-labelled with fluorescent dyes. To image injected hydrogels, photoluminescent hydrogels are necessary. Yet there lacks fast gelling hydrogels that are also photoluminescent.

Current injectable hydrogels with photoluminescence are synthesized by mixing or conjugating hydrogels with semiconducting quantum dots [35,36], carbon dots [34], rare-earth upconversion nanoparticles [37–39], or organic dyes [40–43]. Compared to organic dye conjugated hydrogels, those incorporated with semiconducting quantum dots, carbon dots, and rare-earth upconversion nanoparticles may have toxicity concern [44]. For those organic dye conjugated hydrogels, quick decrease of fluorescent intensity due to photobeleaching is a major obstacle for long term monitoring of hydrogels in vivo [34,44]. Development of hydrogels with low photobeleaching remains a significant challenge.

The objective of this work was to develop injectable, fast gelling, and photoluminescent hydrogels with low photobeleaching. The hydrogels were also thermosensitive. One of the advantages of using thermosensitive hydrogels for stem cell delivery is that gelation process is simply initiated by temperature without using chemical crosslinkers that may raise cytotoxic concerns [45–49]. The hydrogels were synthesized by copolymerization of NIPAAm, HEMA, AOLA, and VP. Conjugation of relatively photostable HYP with PVP component resulted in hydrogels with low photobleaching. Hydrogel injectability, gelation rate, thermal property, mechanical property, degradation, photoluminescence change during degradation, and biocompatibility were evaluated. MSC proliferation and paracrine effects in vitro, and MSC retention in muscle tissue were investigated.

#### 2. Materials and methods

#### 2.1. Materials

NIPAAm and HEMA were purchased from VWR. NIPAAm was recrystallized for 3 times using ethyl acetate and hexane. VP was obtained from Sigma-Aldrich. HEMA and VP were used before passing through a column packed with inhibitor remover. Benzoyl peroxide (Fisher Scientific) and HYP (VWR) were used as received. All solvents were purchased from VWF and used as received.

#### 2.2. Synthesis of hydrogels

The hydrogel polymers were synthesized by free radical polymerization of NIPAAm, HEMA, AOLA, and VP (Scheme 1). AOLA was synthesized by acylation of oligolactide HO-PLA-OCH<sub>3</sub> with acryloyl chloride [45,46]. To synthesize HO-PLA-OCH<sub>3</sub>, D,L-lactide and NaOCH<sub>3</sub> were dissolved in CH<sub>2</sub>Cl<sub>2</sub> and methanol, respectively. The two solutions were then mixed and stirred for 2 h at 0 °C, followed by rinsing with 0.1 M HCl and deionized water [46]. The four components NIPAAm, HEMA, AOLA, and VP were dissolved in 1,4dioxane in a 250 mL three-necked flask with gas inlet and outlet. Two different molar ratios of NIPAAm/HEMA/AOLA/VP were used, i.e., 72/10/8/10 and 67/10/8/15. Benzoyl peroxide (0.2% of the total molar number of monomers) was added into the solution after 15 min of  $N_2$  purging [48,50–53]. The flask was then placed in a preheated oil bath at 65 °C for 24 h. The polymer solution was precipitated in cold hexane. The polymer was purified with THF/ethyl ether twice, and vacuum dried before use. The two polymers are abbreviated as PNHAV10 and PNHAV15 where 10 and 15 represent VP content in the polymers.

#### 2.3. Conjugation of HYP to the hydrogels

The synthesized polymers were dissolved in Dulbecco's modified phosphate-buffered saline (DPBS) to form 10 wt% hydrogel solutions. HYP was then added to the solution at a molar ratio of 6/5 (HYP/polymer). The mixture was stirred overnight at 4 °C for conjugation. Upon gelation at 37 °C, the remaining HYP was removed by dialysis in deionized water for 3 days and the water was changed every 12 h. The two HYP conjugated polymers are abbreviated as PNHAV10HYP and PNHAV15HYP where 10 and 15 represent hydrogels with 10% and 15% of VP, respectively. To confirm the conjugation (Scheme 1), UV-Vis absorption spectra were acquired using a UV-Vis spectrophotometer (Thermo Scientific). The HYP solution and HYP conjugated hydrogel solution in DMSO were placed in a plastic cuvette with an optical path of 1 cm. The spectra were measured in the range of 500 nm and 700 nm [54-56]. Fluorescence spectra were also recorded. The polymer was dissolved in a solution of 5% DMSO in DPBS and emission bands were measured by SpectraMax iD3 spectrometer (Molecular Devices). Excitation wavelength of 480 nm was used.

#### 2.4. Characterization of synthesized photoluminescent hydrogels

Chemical structure of the synthesized polymers was confirmed by  $^1\text{H}$  NMR spectrum. The composition was calculated based on the spectrum. Injectability of the 10 wt% hydrogel solution was tested by injecting the pre-cooled solution (4 °C) through a 26G needle, which is commonly used for injection surgeries [57]. Thermal transition temperature of the solution was measured using Differential Scanning Calorimetry (DSC) in the temperature range of 0 °C and 90 °C at a heating rate of 10 °C/min. The temperature at the maximum endothermal peak was considered as thermal transition temperature. Gelation time of the hydrogel solution was evaluated at

Scheme 1. Synthesis of hydrogel by free radical polymerization, conjugation of hydrogel with hypericin (HYP), and degradation of HYP-conjugated hydrogel.

37 °C using an Olympus microscope (IX71) equipped with a temperature controllable system (Weather Station, Precisioncontrol. Inc.). It is defined as the time for the solution to become completely opaque [47,48,58]. Hydrogel water content as growth factor and cell t was measured after the solid gels were immersed in PBS at 37 °C for 24 h. The gels were then taken out and weighted. Water content was defined as:

 $Water\,content\,(\%)=(w_2-w_1)/w_1\times 100\%$ 

where  $w_1$  and  $w_2$  are mass of the hydrogel at dry and weight states, respectively.

To test mechanical properties, the hydrogel solutions were first solidified at 37 °C overnight. The solid gels were then cut into specimens with sizes of 5 mm  $\times$  5 mm  $\times$  25 mm. Mechanical properties were tested using an Instron tensile tester equipped with a 44.5 N load cell and a 37 °C water bath. Cross-head speed was 50 mm/min. Young's moduli of the hydrogels were calculated from the stress-strain curves using a Matlab program [50–52].

## 2.5. Hydrogel degradation and cytotoxicity of the degradation products

To test hydrogel degradation, 200  $\mu l$  of 10 wt% hydrogel solution was placed in a 1.5 mL microcentrifuge tube, and incubated at 37 °C for 5 h. The supernatant was then taken out, and 200  $\mu l$  of DPBS was added to the tube. The degradation was conducted at 37 °C for 8 weeks. Four samples for each hydrogel type were collected at each time point. The samples were freeze-dried and weighed.

To evaluate cytotoxicity of the degradation product, the final degradation product shown in Scheme 1 was synthesized using the same method as for the hydrogels, and conjugated with HYP. The ratio of NIPAAm/HEMA/AAc/VP was 72/10/8/10. Rat cardiac fibroblasts were seeded in a 96-well tissue culture plate at a den-

sity of  $2\times10^5$  cells/mL, and cultured in a medium containing Dulbecco's modified Eagle's medium (DMEM) and 10% FBS. After 24 h, 50  $\mu$ l of degradation product solution was added to the medium. The control group was cells cultured with the medium without degradation product. After 48 h, cell viability was examined by MTT assay.

#### 2.6. Monitoring of hydrogel fluorescent signal change in vitro

To image hydrogels and detect fluorescent intensity change during hydrogel degradation, 200  $\mu l$  of 4 °C hydrogel solution was placed on a glass slide. After gelation in a 37 °C incubator to form a film, the glass slide was placed in 37 °C DPBS. The DPBS was not replaced at each time point. After 1, 7, 14, 21, and 28 days, the glass slide was taken out to detect fluorescent intensity using a fluorescent plate reader. Four slides for each hydrogel were continuously measured at each time point. In addition, two slides for each hydrogel were continuously imaged at each time point by confocal microscope.

#### 2.7. MSC proliferation and paracrine effects in the hydrogels

Rat bone marrow-derived MSCs were cultured in alpha modified minimum essential medium ( $\alpha$ -MEM) with 10% FBS and 1% antibiotics. Cells used for encapsulation were at passages 10–12. Our previous reports showed that MSCs at these passages remained multipotency [59,60]. Before encapsulation, cells were labeled with live cell tracker CMFDA following the protocol provided by the vendor. To encapsulate MSCs into the hydrogels, cell suspension was placed on ice and mixed with 10 wt% hydrogel solution. The final cell density was 8 million/mL. 200  $\mu$ l of mixture was transferred into each microcentrifugation tube, followed by gelation in a 37 °C incubator for 30 min. After removing the supernatant, 200  $\mu$ l of culture medium was added into each microcen

trifuge tube. The tubes were cultured under normal conditions (21%  $O_2$ , 5%  $CO_2$ , 37 °C) for 2 weeks.

MSC proliferation in the hydrogels was determined by double stranded DNA (dsDNA for live cells) content after 1, 7 and 14 days of culture (n = 4 for each condition at each time point). The samples were washed with DPBS for 3 times and then digested with papain solution at 60 °C for 24 h. The dsDNA content was measured by PicoGreen dsDNA Assay [61]. To image live cells, Olympus Filter FV1000 confocal microscope was used. Z-stack images were collected. To characterize MSC paracrine effects real-time RT-PCR was used to determine gene expressions of growth factors like PDGFB and IGF-1. RNA was first isolated from the hydrogels by TRIzol (SigmaAldrich). The concentration of RNA was evaluated using a Nanodrop system. 1 µg of RNA was utilized for cDNA synthesis using a high-capacity cDNA reverse transcription kit (Applied Biosystem). The primers used were listed in Table 1 [48.52.53]. Real-time RT-PCR was performed with Maxima SYBR Green/Fluorescein master mix on an Applied Biosystem 7900 system. β-Actin was used as a housekeeping gene. A standard  $\triangle\triangle$ Ct method was used to calculate the fold differences.

#### 2.8. Subcutaneous implantation of hydrogels

All animal experiments were conducted in accordance with the National Institutes of Health Guide for handling laboratory animals and the protocol was approved by the Institutional Animal Care and Use Committee of the Ohio State University. C57BL/6 mice aged 8–10 weeks were used. The 10 wt% hydrogel solutions were sterilized under UV light for 30 min. Before injection, the solutions were precooled to 4 °C. Injections were made into the back of each mouse (200 µl/injection and 2 injections/mouse). Two mice were used for each hydrogel type. The mice without injection were served as control. After 4 weeks of injection, tissues were collected and fixed in 4% paraformaldehyde for 48 h. The tissues were then dehydrated, embedded in paraffin, and sectioned into  $4 \mu m$  thick slices. The sections were then stained with H&E. For immunohistological study, the tissue sections were blocked by 3% BSA, permeated with 0.2% Triton X-100, and incubated with primary antibody of F4/80 overnight under 4 °C. After rinsing with PBS, the Alexa fluor 488 secondary antibody was added and incubated for 1 h. Finally. Hoechst was used to counterstain nucleus. Immunofluorescence images were recorded by Olympus Filter FV1000 confocal microscope. The ratio of F4/80 positive cells was quantified from the images.

#### 2.9. Injection of hydrogel and MSCs into thigh muscles

To determine MSC retention in the tissue, CMDil labeled MSCs were first mixed with PBS, collagen (3.5 mg/ml), and hydrogel solutions (10 wt%), respectively. The final cell density was 2 million/ml. The mixtures were then injected into thigh muscles of C57BL/6 mice aged 8–10 weeks (2 injections/hindlimb, 25  $\mu$ l/injection, and 6 hindlimbs for each group). After 24 h, the tissues were harvested, fixed with 4% paraformaldehyde, and frozen sectioned.

**Table 1** Sequences of primers used for real-time RT-PCR.

Gene	Primer Sequences
β-Actin	Forward: AAGATCAAGATCATTGCTCCTC Reverse: GGACTCATCGTACTCCTG
PDGFB	Forward: GATGCCTTGGAGACAAACCTGACA Reverse: ATACTTCTCTTCCTCCTGCGAATGGGC
IGF-1	Forward: TGACATGCCCAAGACTCAGAAGGA Reverse: GGTTGCTCAAGCAGCAAAGGATCT

MSCs retained in the tissues were imaged using Olympus Filter FV1000 confocal microscope. The cell density was quantified as #/mm<sup>2</sup>.

To determine hydrogel fluorescent intensity change and MSC survival after implantation, hydrogel solutions (10 wt%) were mixed with CMDil labeled MSCs (6 million/ml), and injected into thigh muscles of NCr nude mice aged 9 weeks (2 injections/hindlimb, 25  $\mu$ l/injection, 4 hindlimbs were used). After 0, 7, 14, and 28 days, the animals were imaged by In Vivo Imaging System (IVIS) Lumina II with emission filter wavelengths ranging from 575 nm to 650 nm. The tissues were harvested after 28 days, fixed with 4% paraformaldehyde, and frozen sectioned. MSCs in the tissues were imaged using Olympus Filter FV1000 confocal microscope.

#### 2.10. Statistical analysis

Data analysis was performed using ANOVA with post hoc Neuman-Keuls testing. Statistical significance was defined as p < 0.05.

#### 3. Results

#### 3.1. Synthesis of hydrogels and conjugation with HYP

Structure of the synthesized hydrogels was characterized by <sup>1</sup>H NMR spectra. Fig. 1 shows that characteristic peaks for each component were appeared in the spectrum. The ratios of NIPAAm/HEMA/AOLA/VP in the polymers were quantified from <sup>1</sup>H NMR spectra. Table 2 demonstrates that composition of each polymer was consistent with the corresponding feed ratio.

To impart hydrogels with imageability, HYP was conjugated to each hydrogel by forming a complex with VP unit in the polymers. The conjugation was verified by UV–Vis spectra (Fig. 2A). Before conjugation, HYP exhibited two major absorption peaks at 560 and 605 nm, respectively. After conjugation, the two peaks were shifted to 550 nm and 595 nm respectively, likely due to molecular environment change to the HYP. In the fluorescence spectrum, HYP showed two emission bands at 621 nm and 662 nm, respectively (Fig. 2B). The emission band at 621 nm was shifted to 607 nm after HYP was conjugated to the hydrogel. Meanwhile, the band at 662 nm became unpronounced (Fig. 2B).

## 3.2. Hydrogel solution flowability, injectability, thermal transition temperature, and gelation time

The two HYP conjugated copolymers PNHAV10HYP and PNHAV15HYP were able to dissolve in DPBS to form hydrogel solutions at 4 °C. Both solutions were flowable (Fig. 2C), and can be readily injected through a 26G needle (Fig. 2D). Thermal transition temperatures of the hydrogel solutions were measured by DSC and are listed in Table 3. The hydrogel PNHAV10HYP with VP content of 10% exhibited a thermal transition temperature of 21.4 °C. The increase in VP content to 15% (for PNHAV15HYP) augmented the thermal transition temperature to 26.4 °C. The 4 °C hydrogel solutions solidified within 7 s at 37 °C to form opaque gels (Fig. 2E). The gels were stretchable at 37 °C (Fig. 2F and G).

#### 3.3. Hydrogel water content and mechanical properties

Hydrogel water content was determined after the formed gels were incubated in a 37 °C DPBS for 24 h. Table 3 demonstrates that water content was dependent on the VP content in the hydrogels. An increase in VP content from 10% to 15% significantly increased water content from 40% to 69% (p < 0.01).

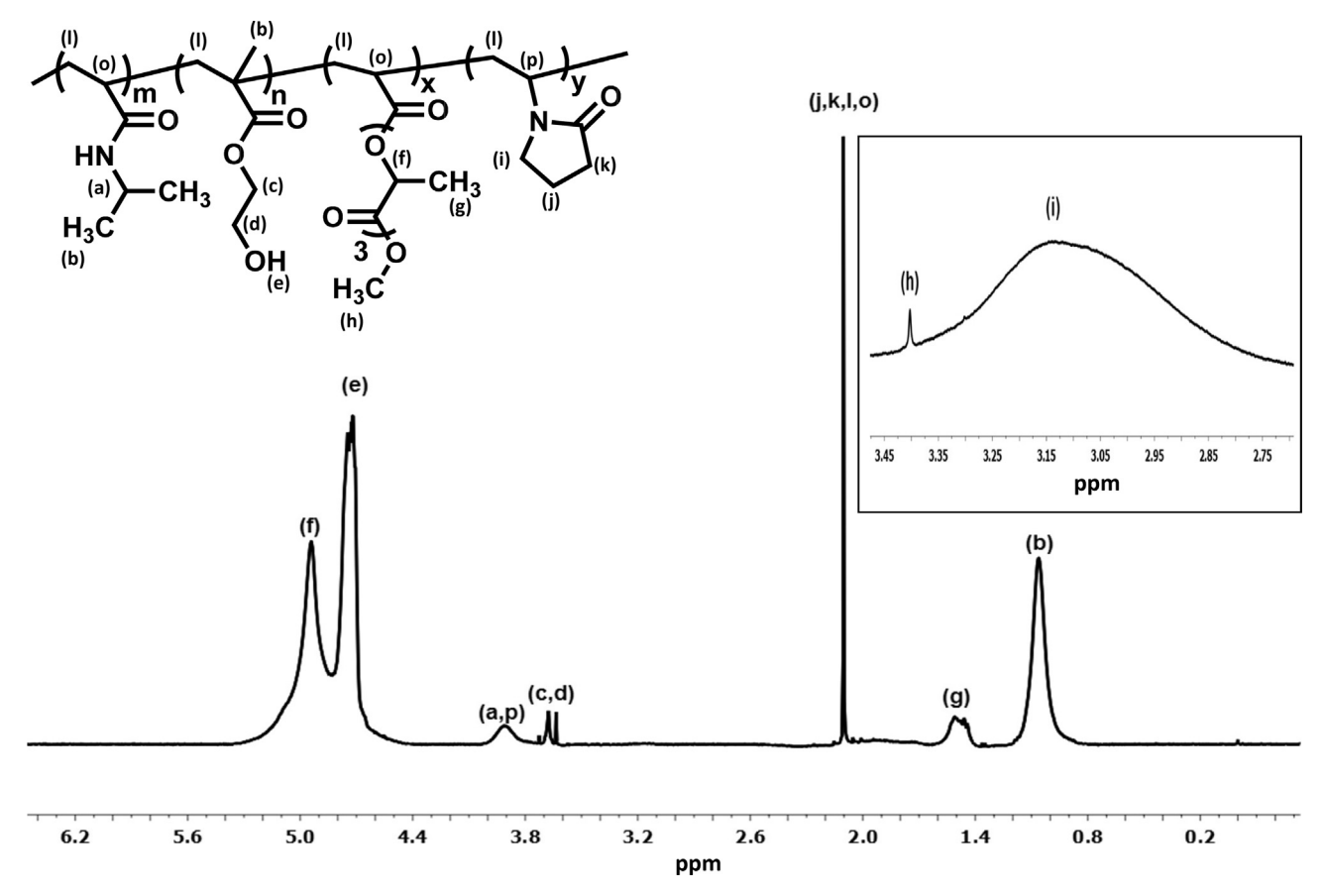


Fig. 1. <sup>1</sup>H NMR spectrum of hydrogel with 10% of VP content (PNHAV10HYP). CDCl<sub>3</sub> was used as solvent.

**Table 2** Hydrogel copolymer feed ratio and composition.

Hydrogel <sup>a</sup>	Feed ratio <sup>b</sup>	Composition <sup>b</sup>
PNHAV10	72/10/8/10	73/10/7/10
PNHAV15	67/10/8/15	65/11/9/15

<sup>&</sup>lt;sup>a</sup> PNHAV10 and PNHAV15 represent hydrogels PNHAV with VP content of 10% and 15%, respectively.

Hydrogel tensile properties were characterized in a 37 °C water bath. Both hydrogels were highly flexible with breaking strains greater than 500%. Typical stress–strain curves for the first 80% of strain are shown in Fig. 3 in order to demonstrate the difference of two hydrogels at the initial stretching stage. The two hydrogels had different tensile behaviors in the first 35% of strain where hydrogel PNHAV10HYP appeared to be softer than hydrogel PNHAV15HYP (Fig. 3). Hydrogel tensile strength and Young's modulus were dependent on the VP content (Table 3). The increase of VP content from 10% to 15% substantially decreased tensile strength from 12.5 kPa to 9.0 kPa (p > 0.05), and significantly reduced Young's modulus from 34.9 kPa to 19.6 kPa (p < 0.01).

#### 3.4. In vitro hydrogel degradation, and fluorescent intensity change

Both hydrogels showed gradual weight loss when incubated in the 37 °C DPBS (Fig. 4A). After 8 weeks of degradation, the hydrogels PNHAV10HYP and PNHAV15HYP remained 83.2% and 76.7% of initial weight, respectively. The weight remaining of PNHAV10-HYP was significantly greater than that of PNHAV15HYP (p < 0.05), suggesting that the hydrogel with higher VP content degraded faster.

Fluorescent signal change during the degradation was monitored for 4 weeks. The fluorescent intensity continuously decreased during the degradation (Fig. 4B). After 4 weeks, the hydrogels PNHAV10HYP and PNHAV15HYP retained 83.7% and 80.1% of the initial fluorescent intensity respectively, and there was no significant difference between the two hydrogels (p > 0.05). The remaining fluorescent intensity for both hydrogels was comparable with their weight remaining. Fluorescent images of the hydrogel PNHAV15HYP at different degradation time confirmed that fluorescent signal became weaker during the degradation (Fig. 4C). The above results demonstrate that hydrogel fluorescent intensity decrease was resulted from hydrogel degradation, and the hydrogels had low photobleaching.

#### 3.5. Cytotoxicity of degradation products

To evaluate cytotoxicity of the final degradation product, fibroblasts were cultured with the supplement of 0, 1, 5, 10, and 15 mg/ml of degradation product, respectively. MTT assay was then performed after 48 h of culture to measure cell viability. All of the groups supplemented with degradation product had similar cell viability as that without degradation product (p > 0.05, Fig. 5), demonstrating that the final degradation product was nontoxic even at a relatively high concentration, 15 mg/ml.

#### 3.6. MSC growth and paracrine effects in the hydrogels

Hydrogels were encapsulated with MSCs to investigate their ability to promote MSC growth and paracrine effects. Live cell number was quantified by dsDNA content. Fig. 6A shows that dsDNA content was increased for both hydrogels during the 14-

b Molar ratio of NIPAAm/HEMA/AOLA/VP.

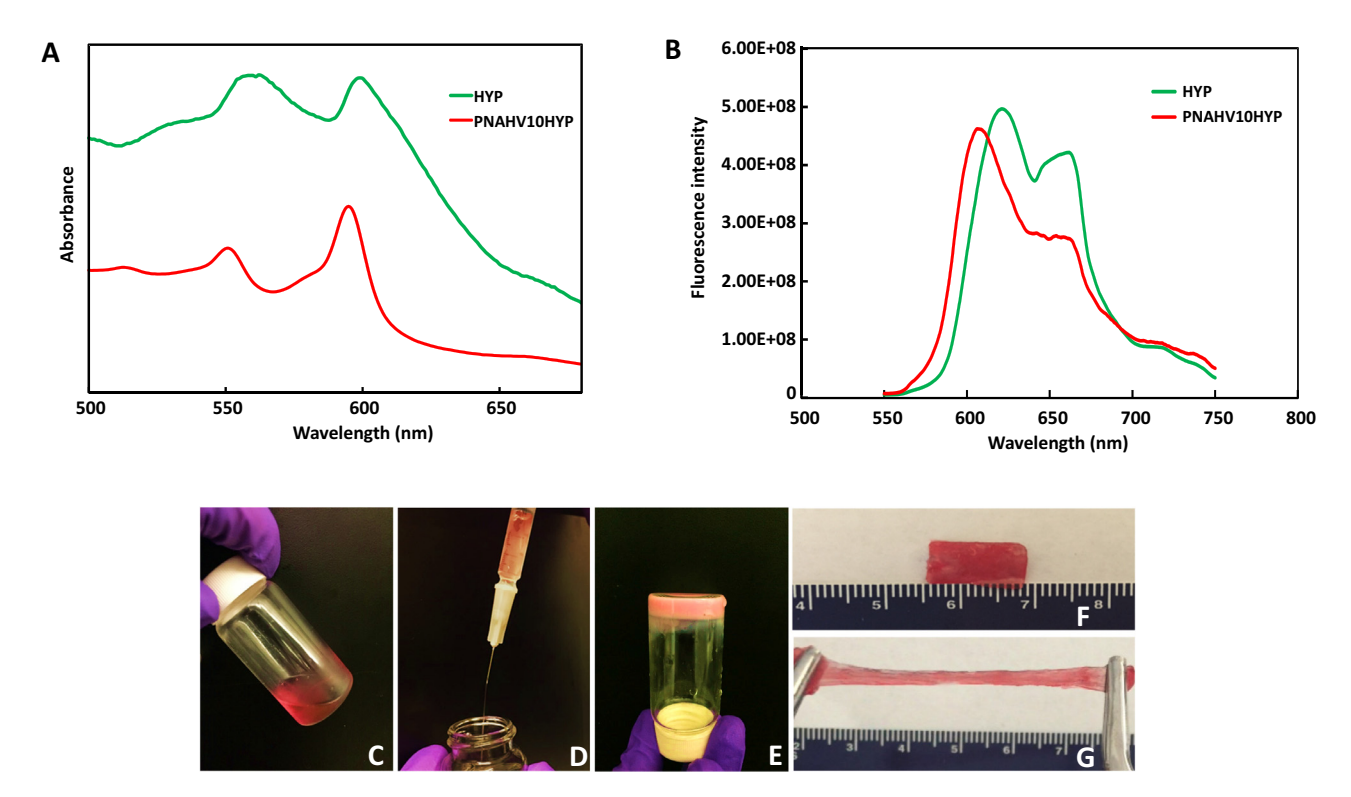


**Fig. 2.** UV–Vis spectra (A) and fluorescence emission spectra (B) of HYP and HYP-conjugated hydrogel. PNHAV10HYP represent HYPconjugated hydrogel PNHAV with VP content of 10%. Flowability, injectability, gelation, and flexibility of HYP-conjugated hydrogel. (C) Hydrogel solution was flowable at 4 °C; (D) 4 °C solution was injectable through a 26-gauge needle; (E) hydrogel solution formed solid gel at 37 °C; (F) Solid gel before stretching at 37 °C; and (G) solid gel after stretching at 37 °C.

**Table 3**Thermal transition temperatures, water content, tensile strengths, and Young's moduli of HYP-conjugated PNHAV hydrogels.

Hydrogel <sup>a</sup>	Thermal transition temperature (°C)	Water content (%)	Tensile strength (kPa)	Young's modulus (kPa)
PNHAV10HYP	21.4	40 ± 3	12.5 ± 2.4	34.9 ± 4.4
PNHAV15HYP	26.4	69 ± 3	$9.0 \pm 1.1$	19.6 ± 3.6

<sup>&</sup>lt;sup>a</sup> PNHAV10HYP and PNHAV15HYP represent HYP-conjugated hydrogels PNHAV with VP content of 10% and 15%, respectively.

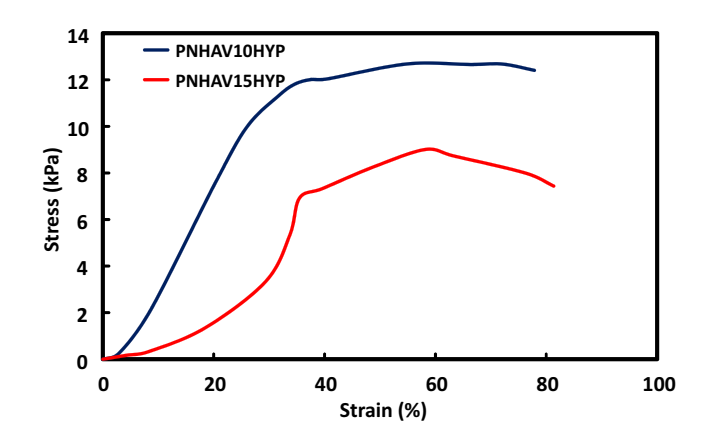


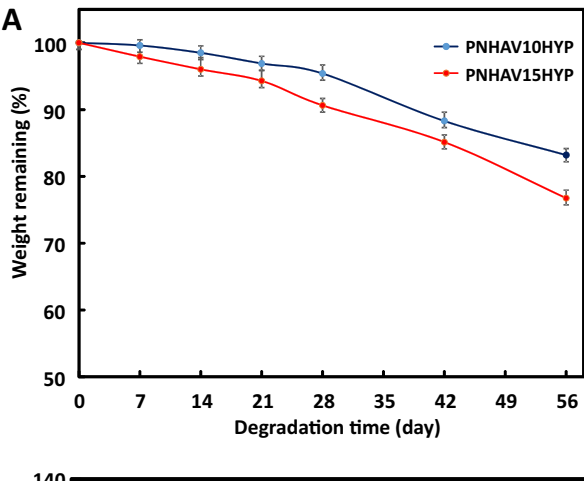
**Fig. 3.** Tensile stress-strain curves of HYP-conjugated hydrogels. PNHAV10HYP and PNHAV15HYP represent HYP-conjugated hydrogels PNHAV with VP content of 10% and 15%, respectively.

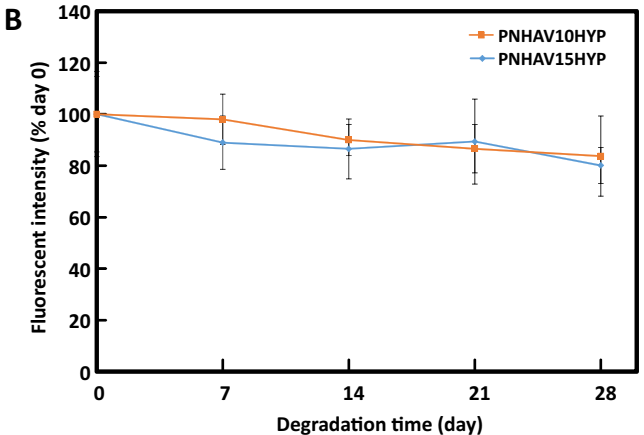
day culture period, indicating that MSCs were able to proliferate in the hydrogels. At days 7 and 14, the hydrogel PNHAV10HYP exhibited substantially greater dsDNA content than the hydrogel PNHAV15HYP (p > 0.05). The dsDNA results were consistent with live cell images, where the cell density was found to increase at days 7 and 14 (Fig. 6B).

MSCs are known to secrete growth factors such as PDGF and IGF-1. These growth factors may promote angiogenesis and cell survival. The effect of the hydrogels on MSC paracrine effects was characterized at the gene level by real time RT-PCR. Fig. 6C shows that the PDGFBB and IGF-1 expressions were significantly increased during the 14-day culture period (p < 0.05 day 14 vs. day 7, day 7 vs. day 1 for each hydrogel). Interestingly at day 14, the IGF-1 expression in the hydrogel PNHAV15HYP was more than 6 times greater than in the hydrogel PNHAV10HYP. These results demonstrate that the developed hydrogels were able to modulate MSC paracrine effects. In future studies we will investigate how the hydrogels affect MSC paracrine effects at the protein level

#### 3.7. Hydrogel in vivo biocompatibility

Hydrogel in vivo biocompatibility was determined after subcutaneous implantation for 28 days. In H&E staining images (Fig. 7A), no obvious inflammation was found for both hydrogel implantation groups compared to the control group without hydrogel implantation. F4/80 staining was performed to determine macrophage content in the control and hydrogel implantation groups (Fig. 7B). Macrophages were appeared in all 3 groups. Further quantification demonstrates that the 3 groups had similar macrophage ratio (Fig. 7C). No significant difference was found among





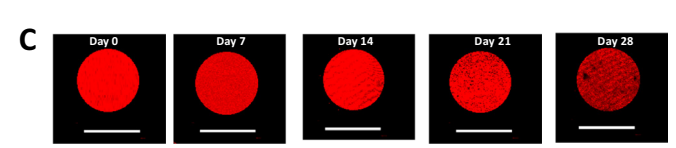


**Fig. 4.** Hydrogel degradation and fluorescence signal change. (A) weight remaining of hydrogels when incubating in PBS at 37 °C for 8 weeks; (B) hydrogel fluorescent intensity change in PBS at 37° C for 4 weeks; and (C) hydrogel fluorescent images during degradation. PNHAV10HYP and PNHAV15HYP represent HYP-conjugated hydrogels PNHAV with VP content of 10% and 15%, respectively.

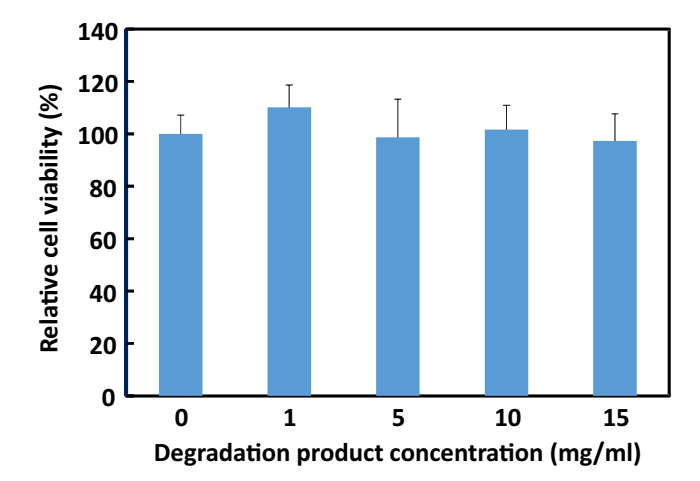


**Fig. 5.** Cell viability of fibroblasts cultured in the medium supplemented with final degradation product. MTT assay was used to quantify cell viability. Cell viability was normalized to the group without adding final degradation product.

the groups (p > 0.05). These results indicate that the hydrogels had excellent biocompatibility.

#### 3.8. Cell retention in thigh muscles when using hydrogel as cell carrier

To determine cell retention in tissue when using fast gelling hydrogel, CMDil labeled MSCs were encapsulated in the solution of hydrogel PNHAV15HYP, and injected into thigh muscles of mice. Cell retention was quantified after 24 h of injection. PBS and collagen solution mixed with MSCs were used as controls. PBS cannot solidify while collagen solution solidified slowly ( $\sim$ 21 min) at 37 °C. Fig. 8A and B demonstrates that the hydrogel significantly increased MSC retention in the muscles compared to collagen and PBS. The cell density in the hydrogel group was  $\sim$ 6.0 times and  $\sim$ 16.9 times of collagen and PBS groups, respectively (p < 0.01, hydrogel vs. collagen, and hydrogel vs. PBS).

### 3.9. Detection of hydrogel fluorescent signal change and MSC survival in vivo

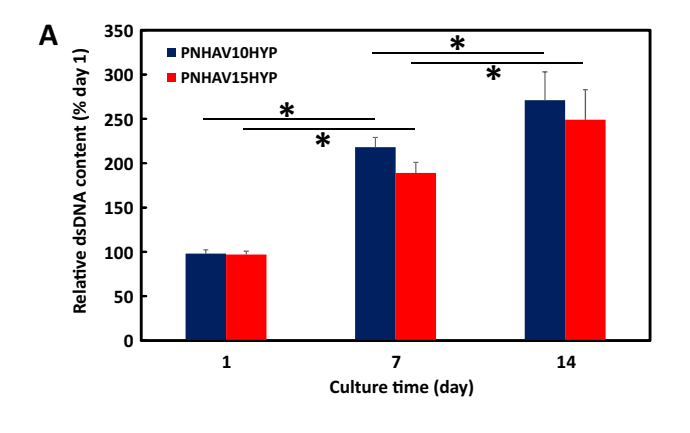
To monitor fluorescent signal change in vivo, the hydrogel PNHAV15HYP encapsulated with CMDil-labeled MSCs was injected into thigh muscles of nude mice. Fluorescent images were then taken at different time points using IVIS system (Fig. 8C).

To image the hydrogel, IVIS emission filter with wavelengths ranging from 575 nm to 650 nm was used. The fluorescent signal of the hydrogel gradually weakened during the 28-day study period. The signal intensity at the edge of the hydrogel decreased more quickly than that in the center, demonstrating that hydrogel degradation was faster on the surface. After 28 days, the hydrogel remained relatively intact with strong intensity remained at the center. This is consistent with in vitro results in Fig. 4B and C. To determine MSC survival in the hydrogel after 28 days of implantation, muscle tissues were imaged. A relatively high density of MSCs was found to survive in the hydrogel (Fig. 8D). This result further demonstrates that the developed hydrogel had good biocompatibility for stem cell delivery into muscles tissues.

#### 4. Discussion

In this work, a family of hydrogels suitable for delivery of stem cells into soft tissues such as infarcted heart and skeletal muscle using a minimally invasive injection approach were developed. The hydrogels were thermosensitive, fast gelling, highly flexible, degradable, and photoluminescent. The thermosensitive and fast gelling hydrogels allow to increase cell retention in the soft tissues as the hydrogels can quickly solidify at 37 °C to prevent leakage of injected hydrogels and encapsulated cells. The hydrogels were highly flexible with mechanical properties similar to those of heart tissue and skeletal muscle. The degradability allows the degradation products to be soluble in body fluid and be removed from the body by urinary system. The photoluminescent property enables to track hydrogel degradation using non-invasive imaging approaches. After the stem cells are delivered into soft tissues, the cells encapsulated in the hydrogels will be gradually released out during hydrogel degradation. Imaging of the hydrogels will inform whether the delivered stem cells are totally released out.

The hydrogels were based on NIPAAm, HEMA, AOLA, and VP. NIPAAm and HEMA were used to introduce hydrogels with thermosensitivity, and to improve water solubility, respectively. AOLA imparted hydrogels with degradability. After hydrolysis of ester bonds, the AOLA unit became acrylic acid unit, which increased not only hydrogel hydrophilicity but also thermal transition temperature above 37 °C so that the degradation products can dissolve in body fluid. VP was responsible for conjugating with HYP by com-



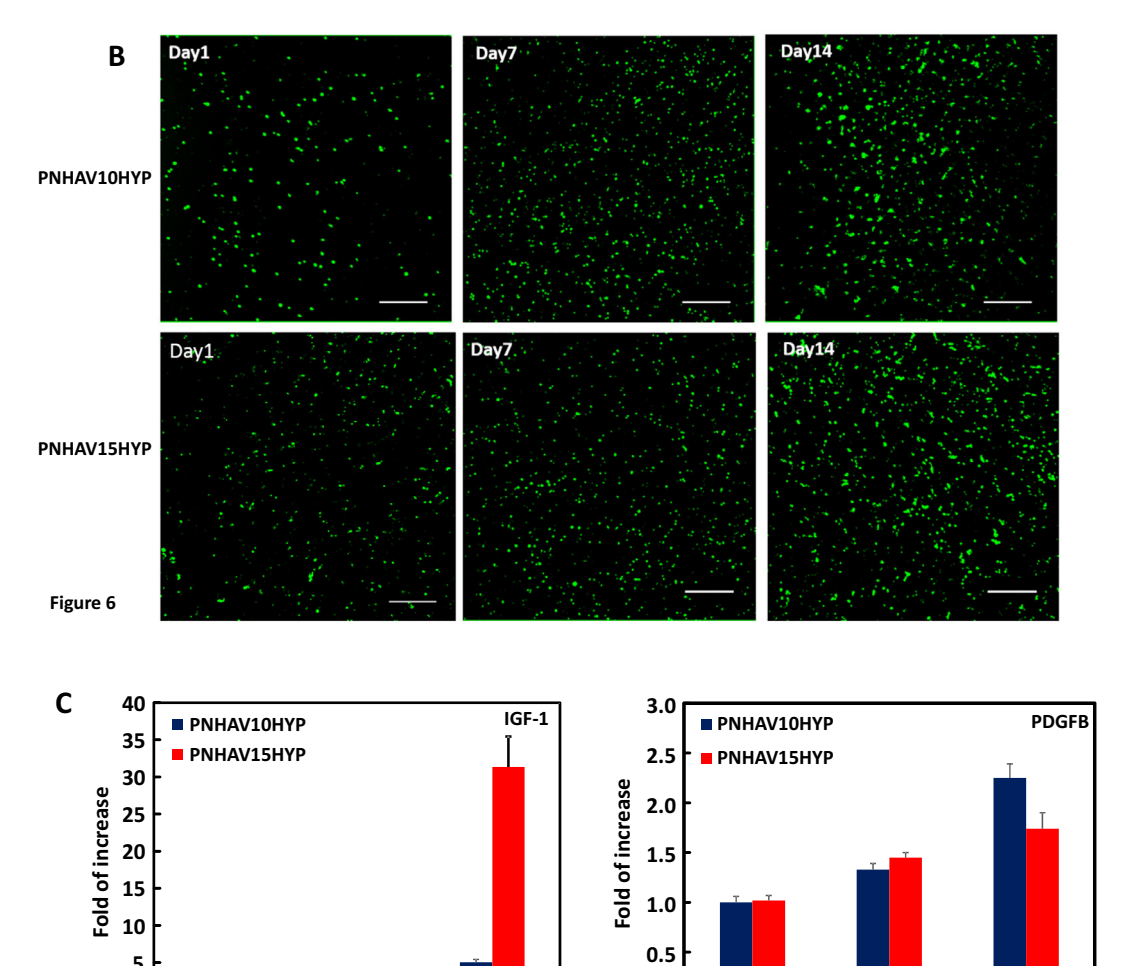


**Fig. 6.** MSC growth in HYP-conjugated hydrogels. (A) dsDNA content of MSCs encapsulated in the hydrogels during 14 days of culture.  $^{\circ}$ p < 0.05; (B) live cell images of MSCs encapsulated in the hydrogels during 14 days of culture period. PNHAV10HYP and PNHAV15HYP represent HYP-conjugated hydrogels PNHAV with VP content of 10% and 15%, respectively. Scale bar = 200  $\mu$ m; (C) Paracrine effects of MSCs encapsulated in HYP-conjugated hydrogels during 14 days of culture. Gene expressions of IGF-1 and PDGFB were determined by real time RT-PCR.

1

14

7

Culture time (day)

plexation. Previous studies have demonstrated that PVP and HYP complex is stable [56,62]. After conjugating with HYP, the hydrogels became fluorescent with a major emission peak at 607 nm (Fig. 2B). Besides its photoluminescent property, HYP has antidepressant, antiviral, and antineoplastic properties [63,64].

1

5 0

The hydrogel solutions were readily injectable at 4 °C using a 26G needle. This type of needle can be used for heart muscle and

skeletal muscle injection [46,64,65]. The hydrogel solutions had thermal transition temperatures around room temperature (Table 3). These solutions can thus solidify at 37 °C. The increase of VP content from 10% to 15% elevated the thermal transition temperature from 21.4 °C to 26.4 °C. This increase is likely the contribution of VP as PVP is highly hydrophilic. Previous studies have demonstrated that copolymerization of NIPAAm with hydrophilic

Culture time (day)

14

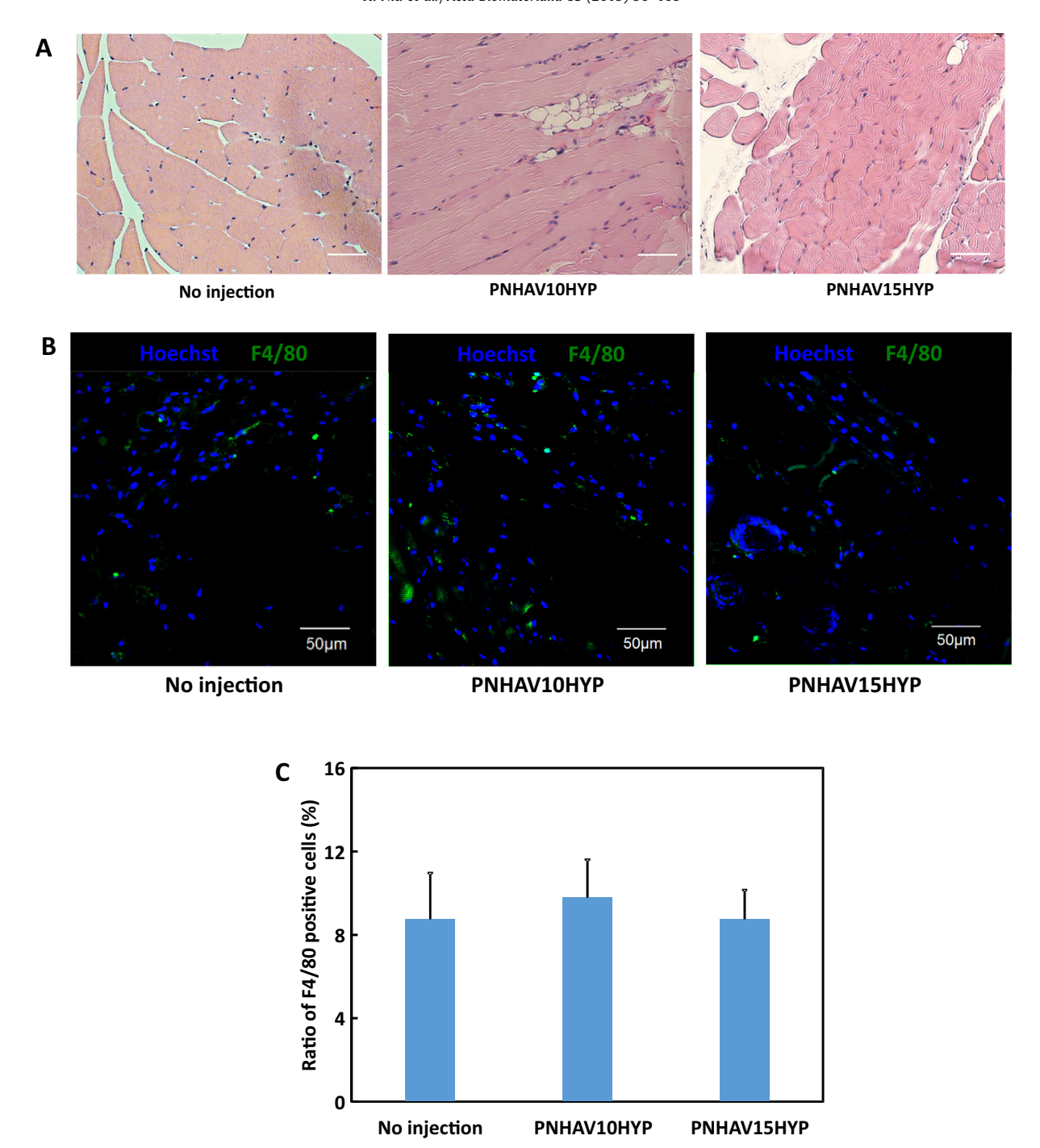


**Fig. 7.** Subcutaneous implantation of hydrogels in C57BL/6 mice. (A) H&E staining images of tissues after subcutaneous implantation for 4 weeks; (B) F4/80 immunofluorescent staining of tissues after subcutaneous implantation for 4 weeks; and (C)) ratio of F4/80 positive cells in tissues. The mice without injection were used as control. PNHAV10HYP and PNHAV15HYP represent HYP-conjugated hydrogels PNHAV with VP content of 10% and 15%, respectively. Scale bar =  $50 \mu m$ .

components like HEMA, acrylic acid, propylacrylic acid, and methacrylic acid can increase thermal transition temperatures of PNIPAAm [47,49,50,66].

The hydrogel solutions were able to solidify within 7 s at 37 °C (Fig. 2E). The gelation time was measured by the turbidity change of hydrogel solution during sol-gel transition in a 37 °C environment. This approach has been established in our previous reports [47,52,53,67,68]. There are other methods can be used to determine gelation time, for example, measurement of rheological properties of polymer solution [69-71], monitoring of polymer solution light transmittance when gradually elevating its temperature [72-

74], tilting a solution at a certain temperature until it finishes gelling [75,76], and pipetting solution up and down at a certain temperature until it cannot pass through a pipette tip [77–79,75,80,81,82]. Among these methods, rheological property measurement has advantage of obtaining additional properties such as storage and loss moduli of the solid gel. When the fast gelling hydrogels are injected into tissues, they quickly solidify, thus increasing the gel and cell retention in the tissues. Injection of stem cells into soft tissues usually experiences leakage due to low viscosity of the delivery medium such as saline and slow gelling hydrogels [3,5,12,13]. This is especially true for heart injection as

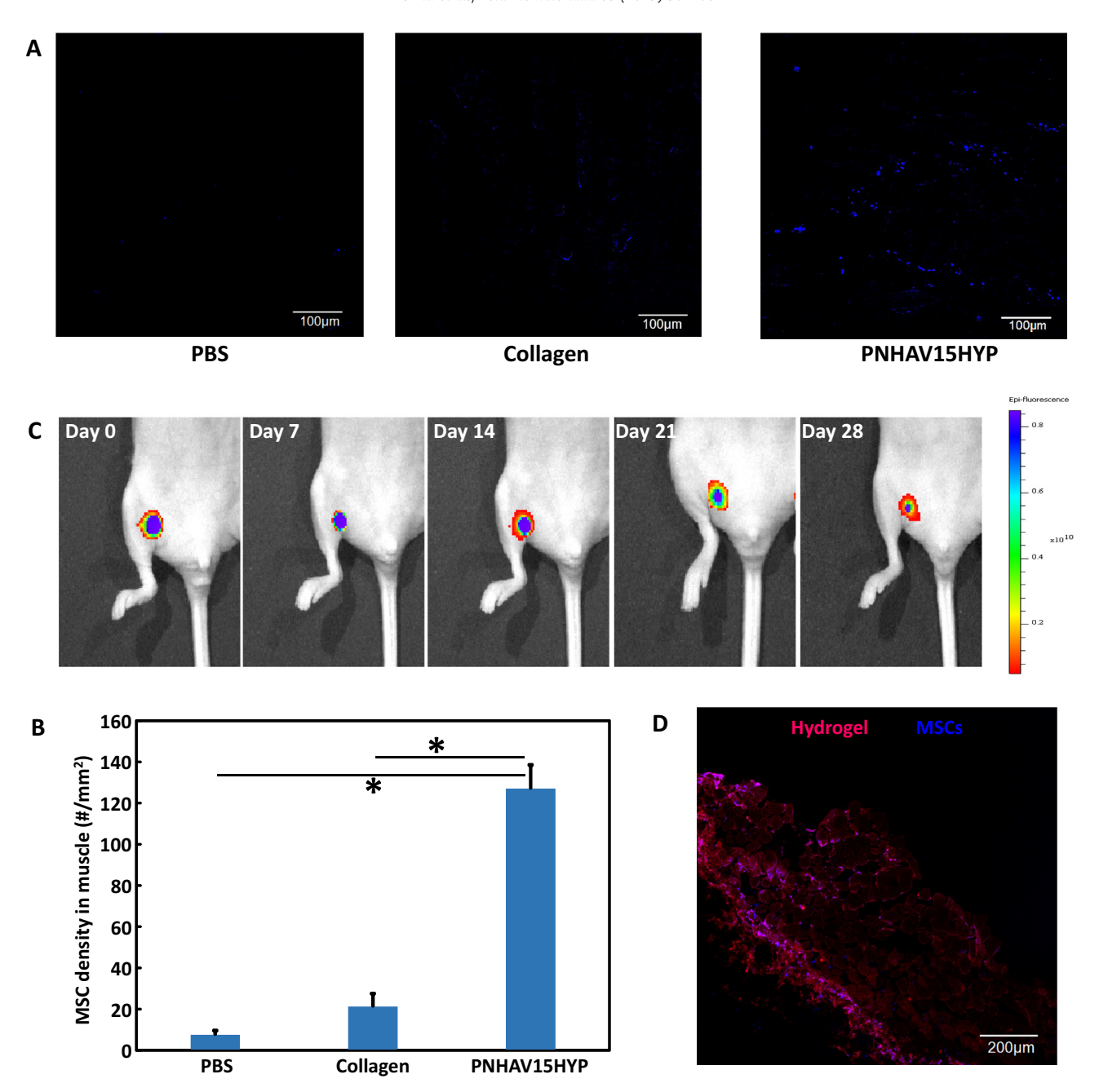


**Fig. 8.** MSC retention in thigh muscles of C57BL/6 mice. MSCs were labeled by live cell tracker CMDil. (A) Live MSCs in muscle tissues after 24 h of implantation. PNHAV15HYP, collagen and PBS were used as cell carriers; (B) quantification of MSC density in tissues based on the images. Scale bar = 100 μm.  $^*p$  < 0.01; Hydrogel fluorescent signal change and MSC survival after injection into thigh muscles of nude mice for 4 weeks. (C) Fluorescent images of hydrogel PNHAV15HYP during the 4-week implantation period; and (D) confocal image of hydrogel and live MSCs (CMDil-labeled) after 4 weeks of implantation. Scale bar = 200 μm. In A and D, the color for red fluorescent CMDil was changed to blue in order to clearly distinguish the CMDil-labeled cells and hydrogel. (For interpretation of the references to color in this figure legend, the reader is referred to the web version of this article.)

the beating heart muscle squeezes out the injected delivery medium. Quick increase of viscosity of the delivery medium upon injection by fast gelation represents one of the strategies to increase cell retention [46,50,66]. Fig. 8B demonstrates that the developed hydrogel significantly increased MSC retention in the muscles compared to slow gelling collagen, and non-gelling PBS. The cell density in the hydrogel group was  $\sim\!6.0$  times and  $\sim\!16.9$  times of collagen and PBS groups, respectively. One of the concerns in using fast gelling hydrogels is that the formed bolus may disrupt electrical conductivity in the heart tissue [83]. However, the hydrogels will be injected into the infarcted region where electrical conductivity is very low. In addition, it is unclear how much disruption of

electrical conductivity will cause heart tissue arrhythmias [46,50,66]. Previous studies using hydrogels with relatively fast gelation rate did not experience obvious arrhythmias. Fast gelling hydrogels will also unlikely block vessels after injecting into ischemic tissues as the injection is typically made in the infarcted region that has extremely low blood flow.

The hydrogels were highly flexible and soft at 37 °C (Figs. 2G, 3 and Table 3). The breaking strains were greater than 500%. The Young's moduli were in the range of 19.6 and 34.9 kPa. These moduli are similar to those of the heart muscle and skeletal muscle [84–86]. Therefore, the hydrogels are suitable for stem cell delivery as they provide native tissue-like mechanical environment for the

delivered cells. After being injected into infarcted hearts, the hydrogels also provide mechanical support to the heart tissue. Following MI, the left ventricular wall stress is gradually increased leading to the decrease of cardiac function [87]. Therefore, the injection of hydrogel with similar modulus as that of the heart tissue may efficiently decrease elevated wall stress to increase cardiac function. Hydrogel Young's modulus was dependent on the VP content. The increase of VP content from 10% to 15% significantly decreased Young's modulus. This is possibly resulted from increased hydrophilicity. The VP units in the hydrogel may decrease the hydrophobic interaction and increase hydrophilic interaction, thus decreasing the chain packing density. This result is consistent with hydrogel water contents (Table 3). It is also in agreement with our previous studies where an increase in hydrophilic interaction decreased the hydrogel Young's modulus [47.67.88].

The developed hydrogels were able to degrade in PBS (Fig. 4A). After 8 weeks of degradation, the weight loss was in the range of 16.8% and 23.3%. The hydrogel with higher VP content exhibited faster degradation rate. This can be attributed to the VP units in the hydrogels as they increased hydrogel water content (Table 3). The degradation is resulted from hydrolysis of oligolactide side chain in the hydrogels. After hydrolysis, the hydrophobic AOLA units become hydrophilic acrylic acid units. This can not only increase hydrophilicity of the final degradation product, but also elevate its thermal transition temperature. We found that the final degradation product for the hydrogel PNHAV10HYP possessed a thermal transition temperature of 38.5 °C. Since this temperature is greater than 37 °C, the degradation product cannot solidify but is soluble at 37  $^{\circ}$ C. In vivo, it will dissolve in body fluid. The final degradation product was non-toxic (Fig. 5). The fibroblast viability did not change even when adding 15 mg/ml of degradation product in the culture medium. In the degradation study, PBS was not changed in the entire study period. Its pH may decrease during the degradation, leading to accelerated hydrolysis.

Hydrogel photoluminescence emission intensity change during degradation was investigated in vitro and in vivo. When the hydrogels were incubated in PBS for 4 weeks, the major emission peak remained at 607 nm. The photoluminescence emission intensity was decreased to 83.7% and 80.1% for hydrogels PNHAV10HYP and PNHAV15HYP, respectively (Fig. 4B). This decrease is solely due to hydrogel degradation instead of photobleaching since the remaining photoluminescence emission intensity was similar or slightly greater than the weight remaining. These results demonstrate that the developed hydrogels had similar photoluminescent property as those degradable polymers with inherent photoluminescence where photoluminescence emission intensity proportionally decreases with polymer weight loss [44]. These results also demonstrate that complexation with the hydrogels allowed HYP to have low photobleaching.

In vivo fluorescent signal change was evaluated after injecting into thigh muscles. The fluorescent intensity progressively decreased during the 4-week study period (Fig. 8C). The in vivo fluorescent intensity decrease was faster than in vitro. This is likely resulted from faster degradation in vivo as proteases may also participate in hydrogel degradation besides water in body fluid. Since the hydrogel retained a relatively strong fluorescent signal at week 4, it is expected that the hydrogel can be detected by imaging for more than 4 weeks. The results will then enable to determine whether the time period for cells to totally release from the hydrogels has effect on the therapeutic efficacy.

To determine in vivo biocompatibility, the hydrogels were implanted subcutaneously for 4 weeks. H&E staining images showed that the hydrogels did not substantially provoke foreign body response compared to the control group without implantation (Fig. 7A). F4/80 staining images demonstrate that the hydrogel

implantation did not induce severe inflammation as the macrophage ratios for the groups with or without hydrogel implantation were similar (Fig. 7B and C). These results suggest that the developed hydrogels had excellent biocompatibility.

To test the effect of hydrogels on stem cell proliferation and paracrine effects, MSCs were encapsulated into both hydrogels and cultured in vitro for 14 days. dsDNA content and live cell imaging demonstrate that MSCs were able to proliferate inside the hydrogels (Fig. 6A and B). These results confirm that the developed hydrogels are suitable for stem cell delivery. MSCs have been used for myocardial infarction therapy and ischemic limb treatment [1,89-92]. Studies have shown that MSCs can improve cardiac function, and promote vascularization in ischemic limbs [1,89-92]. The major contribution of MSCs lies in their paracrine effects which provide multiple growth factors necessary for cell survival and angiogenesis. These growth factors include but are not limited to IGF-1, HGF, bFGF, VEGF, and PDGF [1.89-92]. Approaches that stimulate MSC paracrine effects are attractive as they may increase therapeutic efficacy. In this work, hydrogels PNHAV10HYP and PNHAV15HYP showed different impact on MSC paracrine effects (Fig. 6C). This is likely resulted from difference in hydrogel stiffness as matrix stiffness has been shown to influence MSC paracrine effects [93]. In future studies, we will deliver MSCs and these hydrogels into disease models such as myocardial infarction and limb ischemia to determine MSC survival and proliferation under ischemic conditions, and the effect of MSC paracrine effects on myocardial and skeletal muscle repair and regeneration. The MSCs used in this study represent a model cell type, the hydrogels may also be used to deliver other stem cells. To the best of our knowledge, the hydrogels that not only are photoluminescent, thermosensitive, fast gelling, highly flexible and degradable, but also support stem cell proliferation and paracrine effects, have not been reported previously. One of the limitations of these hydrogels is that the hydrogel shrinkage after gelation may not allow to match the dimension and shape of a particular tissue cavity. Yet the hydrogels can be injected into intact soft tissues together with stem cells for regeneration.

#### 5. Conclusion

In this work, a family of injectable, photoluminescent, thermosensitive, fast gelling, highly flexible and degradable hydrogels were developed for delivery of stem cells into infarcted heart and skeletal muscle tissues. The hydrogels exhibited similar modulus as both tissues. They can be non-invasively monitored by fluorescent imaging, and the signal intensity decreased along with hydrogel degradation. The hydrogels showed good biocompatibility in vitro and in vivo. Interestingly, the hydrogels promoted MSC proliferation and paracrine effects. In addition, the fast gelling hydrogel remarkably increased cell retention in muscle tissues. These hydrogels have potential to not only efficiently deliver stem cells into infarcted heart and skeletal muscle tissues, but also non-invasively track hydrogel degradation and stem cell release from the hydrogel.

#### Acknowledgements

This work was supported by US National Institutes of Health (R01HL138353, R01EB022018, R01AG056919, and R21EB021896), and National Science Foundation (1708956).

#### References

[1] M. Qadura, D.C. Terenzi, S. Verma, M. Al-Omran, D.A. Hess, Cell therapy for critical limb ischemia: an integrated review of pre-clinical and clinical studies, Stem Cells (Dayton, Ohio) (2017).

- [2] A.E. Moran, M.H. Forouzanfar, G.A. Roth, G.A. Mensah, M. Ezzati, A. Flaxman, C. J. Murray, M. Naghavi, The global burden of ischemic heart disease in 1990 and 2010: the global burden of disease 2010 study, Circulation 129 (14) (2014) 1493–1501.
- [3] N.K. Gupta, E.J. Armstrong, S.A. Parikh, The current state of stem cell therapy for peripheral artery disease, Curr. Cardiol. Rep. 16 (2) (2014) 447.
- [4] L. Leroux, B. Descamps, N.F. Tojais, B. Seguy, P. Oses, C. Moreau, D. Daret, Z. Ivanovic, J.M. Boiron, J.M. Lamaziere, P. Dufourcq, T. Couffinhal, C. Duplaa, Hypoxia preconditioned mesenchymal stem cells improve vascular and skeletal muscle fiber regeneration after ischemia through a Wnt4-dependent pathway, Mol. Ther.: J. Am. Soc. Gene Ther. 18 (8) (2010) 1545–1552.
- [5] Y. Li, W. Liu, F. Liu, Y. Zeng, S. Zuo, S. Feng, C. Qi, B. Wang, X. Yan, A. Khademhosseini, J. Bai, Y. Du, Primed 3D injectable microniches enabling low-dosage cell therapy for critical limb ischemia, Proc. Natl. Acad. Sci. U S A 111 (37) (2014) 13511–13516.
- [6] J.S. Janicki, G.L. Brower, J.D. Gardner, A.L. Chancey, J.A. Stewart Jr., The dynamic interaction between matrix metalloproteinase activity and adverse myocardial remodeling, Heart Fail. Rev. 9 (1) (2004) 33–42.
- [7] F.G. Spinale, J.S. Janicki, M.R. Zile, Membrane-associated matrix proteolysis and heart failure, Circ. Res. 112 (1) (2013) 195–208.
- [8] T. Tsuruda, L.C. Costello-Boerrigter, J.C. Burnett Jr., Matrix metalloproteinases: pathways of induction by bioactive molecules, Heart Fail. Rev. 9 (1) (2004) 53–61.
- [9] T.J. Cahill, R.P. Choudhury, P.R. Riley, Heart regeneration and repair after myocardial infarction: translational opportunities for novel therapeutics, Nat. Rev. Drug Discovery 16 (10) (2017) 699–717.
- [10] G. Steinhoff, J. Nesteruk, M. Wolfien, J. Grosse, U. Ruch, P. Vasudevan, P. Muller, Stem cells and heart disease - brake or accelerator?, Adv Drug Deliv. Rev. 120 (2017) 2–24.
- [11] M. Yanamandala, W. Zhu, D.J. Garry, T.J. Kamp, J.M. Hare, H.W. Jun, Y.S. Yoon, N. Bursac, S.D. Prabhu, G.W. Dorn 2nd, R. Bolli, R.N. Kitsis, J. Zhang, Overcoming the roadblocks to cardiac cell therapy using tissue engineering, J. Am. Coll. Cardiol. 70 (6) (2017) 766–775.
- [12] P.K. Gupta, A. Chullikana, R. Parakh, S. Desai, A. Das, S. Gottipamula, S. Krishnamurthy, N. Anthony, A. Pherwani, A.S. Majumdar, A double blind randomized placebo controlled phase I/II study assessing the safety and efficacy of allogeneic bone marrow derived mesenchymal stem cell in critical limb ischemia, J. Transl. Med. 11 (2013) 143.
- [13] E. Benoit, T.F. O'Donnell Jr., M.D. Iafrati, E. Asher, D.F. Bandyk, J.W. Hallett, A.B. Lumsden, G.J. Pearl, S.P. Roddy, K. Vijayaraghavan, A.N. Patel, The role of amputation as an outcome measure in cellular therapy for critical limb ischemia; implications for clinical trial design, J. Transl. Med. 9 (2011) 165.
- [14] X.L. Aranguren, C.M. Verfaillie, A. Luttun, Emerging hurdles in stem cell therapy for peripheral vascular disease, J. Mol. Med. (Berlin, Germany) 87 (1) (2009) 3–16.
- [15] M.K. Mamidi, R. Pal, S. Dey, B.J. Bin Abdullah, Z. Zakaria, M.S. Rao, A.K. Das, Cell therapy in critical limb ischemia: current developments and future progress, Cytotherapy 14 (8) (2012) 902–916.
- [16] G.O. Ouma, B. Zafrir, E.R. Mohler 3rd, M.Y. Flugelman, Therapeutic angiogenesis in critical limb ischemia, Angiology 64 (6) (2013) 466–480.
- [17] K.L. Christman, A.J. Vardanian, Q. Fang, R.E. Sievers, H.H. Fok, R.J. Lee, Injectable fibrin scaffold improves cell transplant survival, reduces infarct expansion, and induces neovasculature formation in ischemic myocardium, J. Am. Coll. Cardiol, 44 (3) (2004) 654–660.
- [18] K.L. Christman, R.J. Lee, Biomaterials for the treatment of myocardial infarction, J. Am. Coll. Cardiol. 48 (5) (2006) 907–913.
  [19] L.M. Ricles, P.L. Hsieh, N. Dana, V. Rybalko, C. Kraynak, R.P. Farrar, L.J. Suggs,
- [19] L.M. Ricles, P.L. Hsieh, N. Dana, V. Rybalko, C. Kraynak, R.P. Farrar, L.J. Suggs, Therapeutic assessment of mesenchymal stem cells delivered within a PEGylated fibrin gel following an ischemic injury, Biomaterials 102 (2016) 9-19.
- [20] R.G. Gomez-Mauricio, A. Acarregui, F.M. Sanchez-Margallo, V. Crisostomo, I. Gallo, R.M. Hernandez, J.L. Pedraz, G. Orive, M.F. Martin-Cancho, A preliminary approach to the repair of myocardial infarction using adipose tissue-derived stem cells encapsulated in magnetic resonance-labelled alginate microspheres in a porcine model, Eur. J. Pharmaceutics and Biopharm.: Off. J. Arbeitsgemeinschaft Fur Pharmazeutische Verfahrenstechnik e.V 84 (1) (2013) 29–39.
- [21] E.T. Roche, C.L. Hastings, S.A. Lewin, D.E. Shvartsman, Y. Brudno, N.V. Vasilyev, F.J. O'Brien, C.J. Walsh, G.P. Duffy, D.J. Mooney, Comparison of biomaterial delivery vehicles for improving acute retention of stem cells in the infarcted heart, Biomaterials 35 (25) (2014) 6850–6858.
- [22] N. Landa, L. Miller, M.S. Feinberg, R. Holbova, M. Shachar, I. Freeman, S. Cohen, J. Leor, Effect of injectable alginate implant on cardiac remodeling and function after recent and old infarcts in rat, Circulation 117 (11) (2008) 1388– 1396.
- [23] P.H. Kim, H.G. Yim, Y.J. Choi, B.J. Kang, J. Kim, S.M. Kwon, B.S. Kim, N.S. Hwang, J.Y. Cho, Injectable multifunctional microgel encapsulating outgrowth endothelial cells and growth factors for enhanced neovascularization, J. Controlled Release: Off. J. Controlled Release Soc. 187 (2014) 1–13.
- [24] W. Dai, L.E. Wold, J.S. Dow, R.A. Kloner, Thickening of the infarcted wall by collagen injection improves left ventricular function in rats: a novel approach to preserve cardiac function after myocardial infarction, J. Am. Coll. Cardiol. 46 (4) (2005) 714–719.
- [25] E.J. Suuronen, J.P. Veinot, S. Wong, V. Kapila, J. Price, M. Griffith, T.G. Mesana, M. Ruel, Tissue-engineered injectable collagen-based matrices for improved cell delivery and vascularization of ischemic tissue using CD133+ progenitors

- expanded from the peripheral blood, Circulation 114 (1 Suppl) (2006) I138-I144
- [26] C. Xu, M.S. Inokuma, J. Denham, K. Golds, P. Kundu, J.D. Gold, M.K. Carpenter, Feeder-free growth of undifferentiated human embryonic stem cells, Nat. Biotechnol. 19 (10) (2001) 971–974.
- [27] C.Y. Chang, A.T. Chan, P.A. Armstrong, H.C. Luo, T. Higuchi, I.A. Strehin, S. Vakrou, X. Lin, S.N. Brown, B. O'Rourke, T.P. Abraham, R.L. Wahl, C.J. Steenbergen, J.H. Elisseeff, M.R. Abraham, Hyaluronic acid-human blood hydrogels for stem cell transplantation, Biomaterials 33 (32) (2012) 8026–8033.
- [28] H.J. Park, Y. Jin, J. Shin, K. Yang, C. Lee, H.S. Yang, S.W. Cho, Catechol-functionalized hyaluronic acid hydrogels enhance angiogenesis and osteogenesis of human adipose-derived stem cells in critical tissue defects, Biomacromolecules 17 (6) (2016) 1939–1948.
- [29] M. Ishihara, K. Nakanishi, K. Ono, M. Sato, M. Kikuchi, Y. Saito, H. Yura, T. Matsui, H. Hattori, M. Uenoyama, A. Kurita, Photocrosslinkable chitosan as a dressing for wound occlusion and accelerator in healing process, Biomaterials 23 (3) (2002) 833–840.
- [30] S.B. Seif-Naraghi, J.M. Singelyn, M.A. Salvatore, K.G. Osborn, J.J. Wang, U. Sampat, O.L. Kwan, G.M. Strachan, J. Wong, P.J. Schup-Magoffin, R.L. Braden, K. Bartels, J.A. DeQuach, M. Preul, A.M. Kinsey, A.N. DeMaria, N. Dib, K.L. Christman, Safety and efficacy of an injectable extracellular matrix hydrogel for treating myocardial infarction, Sci. Transl. Med. 5 (173) (2013). 173ra25.
- [31] J.A. DeQuach, J.E. Lin, C. Cam, D. Hu, M.A. Salvatore, F. Sheikh, K.L. Christman, Injectable skeletal muscle matrix hydrogel promotes neovascularization and muscle cell infiltration in a hindlimb ischemia model, Eur. Cells Mater. 23 (2012) 400–412. discussion 412.
- [32] J.L. Ungerleider, T.D. Johnson, M.J. Hernandez, D.I. Elhag, R.L. Braden, M. Dzieciatkowska, K.G. Osborn, K.C. Hansen, E. Mahmud, K.L. Christman, Extracellular matrix hydrogel promotes tissue remodeling, arteriogenesis, and perfusion in a rat hindlimb ischemia model, JACC Basic Transl. Sci. 1 (1-2) (2016) 32–44.
- [33] X.J. Jiang, T. Wang, X.Y. Li, D.Q. Wu, Z.B. Zheng, J.F. Zhang, J.L. Chen, B. Peng, H. Jiang, C. Huang, X.Z. Zhang, Injection of a novel synthetic hydrogel preserves left ventricle function after myocardial infarction, J. Biomed. Mater. Res. Part A 90 (2) (2009) 472–477.
- [34] L. Wang, B. Li, F. Xu, Y. Li, Z. Xu, D. Wei, Y. Feng, Y. Wang, D. Jia, Y. Zhou, Visual in vivo degradation of injectable hydrogel by real-time and non-invasive tracking using carbon nanodots as fluorescent indicator, Biomaterials 145 (2017) 192–206.
- [35] M. Franke, S. Leubner, A. Dubavik, A. George, T. Savchenko, C. Pini, P. Frank, D. Melnikau, Y. Rakovich, N. Gaponik, A. Eychmuller, A. Richter, Immobilization of pH-sensitive CdTe quantum dots in a poly(acrylate) hydrogel for microfluidic applications, Nanoscale Res. Lett. 12 (1) (2017) 314.
- [36] J.H. Kim, S.Y. Lim, D.H. Nam, J. Ryu, S.H. Ku, C.B. Park, Self-assembled, photoluminescent peptide hydrogel as a versatile platform for enzyme-based optical biosensors, Biosens, Bioelectron, 26 (5) (2011) 1860–1865.
- [37] J.Y.R. Silva, L.L. da Luz, F.G.M. Mauricio, I.B. Vasconcelos Alves, J.N.S. Ferro, E. Barreto, I.T. Weber, W.M. de Azevedo, S.A. Junior, Lanthanide-organic gels as a multifunctional supramolecular smart Platform, ACS Appl. Mater. Interfaces 9 (19) (2017) 16458–16465.
- [38] G. Jalani, R. Naccache, D.H. Rosenzweig, S. Lerouge, L. Haglund, F. Vetrone, M. Cerruti, Real-time, non-invasive monitoring of hydrogel degradation using LiYF4:Yb(3+)/Tm(3+) NIR-to-NIR upconverting nanoparticles, Nanoscale 7 (26) (2015) 11255–11262.
- [39] M. Wang, X. Li, W. Hua, L. Shen, X. Yu, X. Wang, Electrospun poly(acrylic acid)/ silica hydrogel nanofibers scaffold for highly efficient adsorption of lanthanide ions and its photoluminescence performance, ACS Appl. Mater. Interfaces 8 (36) (2016) 23995–24007.
- [40] W.W. Wang, J.J. Liu, C. Li, J. Zhang, J.F. Liu, A.J. Dong, D.L. Kong, Real-time and non-invasive fluorescence tracking of in vivo degradation of the thermosensitive PEGlyated polyester hydrogel, J. Mat. Chem. B 2 (26) (2014) 4185–4192.
- [41] N. Artzi, N. Oliva, C. Puron, S. Shitreet, S. Artzi, A. Bon Ramos, A. Groothuis, G. Sahagian, E.R. Edelman, In vivo and in vitro tracking of erosion in biodegradable materials using non-invasive fluorescence imaging, Nat. Mater. 10 (9) (2011) 704–709.
- [42] Y. Zhang, F. Rossi, S. Papa, M.B. Violatto, P. Bigini, M. Sorbona, F. Redaelli, P. Veglianese, J. Hilborn, D.A. Ossipov, Non-invasive in vitro and in vivo monitoring of degradation of fluorescently labeled hyaluronan hydrogels for tissue engineering applications, Acta Biomater. 30 (2016) 188–198.
- [43] X. Dong, C. Wei, T. Liu, F. Lv, Z. Qian, Real-time fluorescence tracking of protoporphyrin incorporated thermosensitive hydrogel and its drug release in vivo, ACS Appl. Mater. Interfaces 8 (8) (2016) 5104–5113.
- [44] J. Hu, J. Guo, Z. Xie, D. Shan, E. Gerhard, G. Qian, J. Yang, Fluorescence imaging enabled poly(lactide-co-glycolide), Acta Biomater. 29 (2016) 307–319.
- [45] Z. Ma, D.M. Nelson, Y. Hong, W.R. Wagner, Thermally responsive injectable hydrogel incorporating methacrylate-polylactide for hydrolytic lability, Biomacromolecules 11 (7) (2010) 1873–1881.
- [46] Z. Fan, M. Fu, Z. Xu, B. Zhang, Z. Li, H. Li, X. Zhou, X. Liu, Y. Duan, P.H. Lin, P. Duann, X. Xie, J. Ma, Z. Liu, J. Guan, Sustained release of a peptide-based matrix metalloproteinase-2 inhibitor to attenuate adverse cardiac remodeling and improve cardiac function following myocardial infarction, Biomacromolecules 18 (9) (2017) 2820–2829.
- [47] Z.F. Zhenqing Li, Xu Yanyi, Wilson Lo, Xi Wang, Hong Niu, Xiaofei Li, Xiaoyun Xie, Mahmood Khan, Jianjun Guan, pH-sensitive and thermosensitive

- hydrogels as stem-cell carriers for cardiac therapy, ACS Appl. Mater. Interfaces 8 (17) (2016) 10752–10760.
- [48] Z. Li, Z. Fan, Y. Xu, H. Niu, X. Xie, Z. Liu, J. Guan, Thermosensitive and highly flexible hydrogels capable of stimulating cardiac differentiation of cardiosphere-derived cells under static and dynamic mechanical training conditions, ACS Appl. Mater. Interfaces 8 (25) (2016) 15948–15957.
- [49] Y.Y. Xu, Z.Q. Li, X.F. Li, Z.B. Fan, Z.G. Liu, X.Y. Xie, J.J. Guan, Regulating myogenic differentiation of mesenchymal stem cells using thermosensitive hydrogels, Acta Biomater. 26 (2015) 23–33.
- [50] K.L. Fujimoto, Z.W. Ma, D.M. Nelson, R. Hashizume, J.J. Guan, K. Tobita, W.R. Wagner, Synthesis, characterization and therapeutic efficacy of a biodegradable, thermoresponsive hydrogel designed for application in chronic infarcted myocardium, Biomaterials 30 (26) (2009) 4357–4368.
- [51] X.G.Z. Li, J. Guan, An oxygen release system to augment cardiac progenitor cell survival and differentiation under hypoxic condition, Biomaterials 33 (25) (2012) 5914–5923.
- [52] Z.Q. Li, X.L. Guo, J.J. Guan, A Thermosensitive hydrogel capable of releasing bFGF for enhanced differentiation of mesenchymal stem cell into cardiomyocyte-like cells under ischemic conditions, Biomacromolecules 13 (6) (2012) 1956–1964.
- [53] Z.Q. Li, X.L. Guo, A.F. Palmer, H. Das, J.J. Guan, High-efficiency matrix modulusinduced cardiac differentiation of human mesenchymal stem cells inside a thermosensitive hydrogel, Acta Biomater. 8 (10) (2012) 3586–3595.
- [54] H. Koren, G. Schenk, R. Iindra, G. Alth, R. Ebermann, A. Kubin, G. Koderhold, M. Kreitner, Hypericin in phototherapy, J. Photochem. Photobiol. B 36 (2) (1996) 113–119.
- [55] A. Kubin, H. Loew, U. Burner, G. Jessner, H. Kolbabek, F. Wierrani, How to make hypericin water-soluble, Die Pharmazie-Int. J. Pharm. Sci. 63 (4) (2008) 263– 269
- [56] A. Kubin, P. Meissner, F. Wierrani, U. Burner, A. Bodenteich, A. Pytel, N. Schmeller, Fluorescence diagnosis of bladder cancer with new water soluble hypericin bound to polyvinylpyrrolidone: PVP-hypericin, Photochem. Photobiol. 84 (6) (2008) 1560–1563.
- [57] H.A. Aliyar, P.D. Hamilton, N. Ravi, Refilling of ocular lens capsule with copolymeric hydrogel containing reversible disulfide, Biomacromolecules 6 (1) (2005) 204–211.
- [58] Ž.X. Zhaobo Fan, Hong Niu, Ning Gao, Ya Guan, Li Chao, Yu Dang, Xiaoyu Cui, Xuanyou Liu Liu, Yunyan Duan, Haichang Li, Xinyu Zhou, Pei-Hui Lin, Jianjie Ma, Jianjun Guan, An injectable oxygen release system to augment cell survival and promote cardiac repair following myocardial infarction, Sci. Rep. 8 (1) (2018).
- [59] Z. Ahmed, E.A. Gooding, K.V. Pimenov, L. Wang, S.A. Asher, UV resonance Raman determination of molecular mechanism of poly (Nisopropylacrylamide) volume phase transition, J. Phys. Chem. B 113 (13) (2009) 4248–4256.
- [60] J.C. Garbern, E. Minami, P.S. Stayton, C.E. Murry, Delivery of basic fibroblast growth factor with a pH-responsive, injectable hydrogel to improve angiogenesis in infarcted myocardium, Biomaterials 32 (9) (2011) 2407–2416.
- [61] D.M. Hoganson, E.M. O'Doherty, G.E. Owens, D.O. Harilal, S.M. Goldman, C.M. Bowley, C.M. Neville, R.T. Kronengold, J.P. Vacanti, The retention of extracellular matrix proteins and angiogenic and mitogenic cytokines in a decellularized porcine dermis, Biomaterials 31 (26) (2010) 6730–6737.
- [62] R. Penjweini, H.G. Loew, P. Breit, K.W. Kratky, Optimizing the antitumor selectivity of PVP-Hypericin re A549 cancer cells and HLF normal cells through pulsed blue light, Photodiagn. Photodyn. Ther. 10 (4) (2013) 591–599.
- [63] Z. Jendželovská, R. Jendželovský, B. Kuchárová, P. Fedoročko, Hypericin in the light and in the dark: two sides of the same coin, Front. Plant Sci. 7 (2016) 560.
- [64] H.N. Murthy, Y.-S. Kim, S.-Y. Park, K.-Y. Paek, Hypericins: biotechnological production from cell and organ cultures, Appl. Microbiol. Biotechnol. 98 (22) (2014) 9187–9198.
- [65] S. Matsushita, J.S. Forrester, C. Li, M. Sato, Z. Li, X. Guo, J. Guan, A. Amano, Administration of cells with thermosensitive hydrogel enhances the functional recovery in ischemic rat heart, J. Tissue Eng. 7 (2016), 2041731416646676.
- [66] Y. Zhu, H. Jiang, S.-H. Ye, T. Yoshizumi, W.R. Wagner, Tailoring the degradation rates of thermally responsive hydrogels designed for soft tissue injection by varying the autocatalytic potential, Biomaterials 53 (2015) 484–493.
- [67] Z. Li, F. Wang, S. Roy, C.K. Sen, J. Guan, Injectable, highly flexible, and thermosensitive hydrogels capable of delivering superoxide dismutase, Biomacromolecules 10 (12) (2009) 3306–3316.
- [68] F. Wang, Z. Li, M. Khan, K. Tamama, P. Kuppusamy, W.R. Wagner, C.K. Sen, J. Guan, Injectable, rapid gelling and highly flexible hydrogel composites as growth factor and cell carriers, Acta Biomater. 6 (6) (2010) 1978–1991.
- [69] A.I. Van Den Bulcke, B. Bogdanov, N. De Rooze, E.H. Schacht, M. Cornelissen, H. Berghmans, Structural and rheological properties of methacrylamide modified gelatin hydrogels, Biomacromolecules 1 (1) (2000) 31–38.

- [70] C. Yan, D.J. Pochan, Rheological properties of peptide-based hydrogels for biomedical and other applications, Chem. Soc. Rev. 39 (9) (2010) 3528– 3540.
- [71] J. Lucey, P. Munro, H. Singh, Effects of heat treatment and whey protein addition on the rheological properties and structure of acid skim milk gels, Int. Dairy I. 9 (3–6) (1999) 275–279.
- [72] S.M. Silva, F.V. Pinto, F.E. Antunes, M.G. Miguel, J.J. Sousa, A.A. Pais, Aggregation and gelation in hydroxypropylmethyl cellulose aqueous solutions, J. Colloid Interface Sci. 327 (2) (2008) 333–340.
- [73] H. Takeshita, T. Kanaya, K. Nishida, K. Kaji, Gelation process and phase separation of PVA solutions as studied by a light scattering technique, Macromolecules 32 (23) (1999) 7815–7819.
- [74] C. Chang, L. Zhang, J. Zhou, L. Zhang, J.F. Kennedy, Structure and properties of hydrogels prepared from cellulose in NaOH/urea aqueous solutions, Carbohydr. Polym. 82 (1) (2010) 122–127.
- [75] D. Gupta, C.H. Tator, M.S. Shoichet, Fast-gelling injectable blend of hyaluronan and methylcellulose for intrathecal, localized delivery to the injured spinal cord, Biomaterials 27 (11) (2006) 2370–2379.
- [76] M.K. Bain, B. Bhowmick, D. Maity, D. Mondal, M.M.R. Mollick, D. Rana, D. Chattopadhyay, Synergistic effect of salt mixture on the gelation temperature and morphology of methylcellulose hydrogel, Int. J. Biol. Macromol. 51 (5) (2012) 831–836.
- [77] N.E. Davis, S. Ding, R.E. Forster, D.M. Pinkas, A.E. Barron, Modular enzymatically crosslinked protein polymer hydrogels for in situ gelation, Biomaterials 31 (28) (2010) 7288–7297.
- [78] A. Jain, Y.-T. Kim, R.J. McKeon, R.V. Bellamkonda, In situ gelling hydrogels for conformal repair of spinal cord defects, and local delivery of BDNF after spinal cord injury, Biomaterials 27 (3) (2006) 497–504.
- [79] A.K. Ekenseair, K.W. Boere, S.N. Tzouanas, T.N. Vo, F.K. Kasper, A.G. Mikos, Structure-property evaluation of thermally and chemically gelling injectable hydrogels for tissue engineering, Biomacromolecules 13 (9) (2012) 2821– 2830.
- [80] E. Cheng, Y. Xing, P. Chen, Y. Yang, Y. Sun, D. Zhou, L. Xu, Q. Fan, D. Liu, A pH-triggered, fast-responding DNA hydrogel, Angew. Chem. 121 (41) (2009) 7796–7799.
- [81] M.D. Baumann, C.E. Kang, J.C. Stanwick, Y. Wang, H. Kim, Y. Lapitsky, M.S. Shoichet, An injectable drug delivery platform for sustained combination therapy, J. Controlled Release 138 (3) (2009) 205–213.
- [82] H. Winter, Can the gel point of a cross-linking polymer be detected by the G'-G"crossover?, Polym Eng. Sci. 27 (22) (1987) 1698–1702.
- [83] S.L. Suarez, A.A. Rane, A. Muñoz, A.T. Wright, S.X. Zhang, R.L. Braden, A. Almutairi, A.D. McCulloch, K.L. Christman, Intramyocardial injection of hydrogel with high interstitial spread does not impact action potential propagation, Acta Biomater. 26 (2015) 13–22.
- [84] A.M. Collinsworth, S. Zhang, W.E. Kraus, G.A. Truskey, Apparent elastic modulus and hysteresis of skeletal muscle cells throughout differentiation, Am. J. Physiol. Cell Physiol. 283 (4) (2002) C1219–C1227.
- [85] B. Bhana, R.K. Iyer, W.L.K. Chen, R. Zhao, K.L. Sider, M. Likhitpanichkul, C.A. Simmons, M. Radisic, Influence of substrate stiffness on the phenotype of heart cells, Biotechnol. Bioeng. 105 (6) (2010) 1148–1160.
- [86] S. Al-Haque, J.W. Miklas, N. Feric, L.L. Chiu, W.L.K. Chen, C.A. Simmons, M. Radisic, Hydrogel substrate stiffness and topography interact to induce contact guidance in cardiac fibroblasts, Macromol. Biosci. 12 (10) (2012) 1342–1353.
- [87] S.T. Wall, J.C. Walker, K.E. Healy, M.B. Ratcliffe, J.M. Guccione, Theoretical impact of the injection of material into the myocardium: a finite element model simulation, Circulation 114 (24) (2006) 2627–2635.
- [88] J. Guan, Y. Hong, Z. Ma, W.R. Wagner, Protein-reactive, thermoresponsive copolymers with high flexibility and biodegradability, Biomacromolecules 9 (4) (2008) 1283–1292.
- [89] C. Miao, M. Lei, W. Hu, S. Han, Q. Wang, A brief review: the therapeutic potential of bone marrow mesenchymal stem cells in myocardial infarction, Stem Cell Res. Ther. 8 (1) (2017) 242.
- [90] A.E.S. Shafei, M.A. Ali, H.G. Ghanem, A.I. Shehata, A.A. Abdelgawad, H.R. Handal, K.A. Talaat, A.E. Ashaal, R. Mostafa, A.S. El-Shal, Mesenchymal stem cells therapy: a promising cell based therapy for treatment of myocardial infraction. J. Cell. Biochem. (2017).
- [91] Y. Fujita, A. Kawamoto, Stem cell-based peripheral vascular regeneration, Adv. Drug Deliv. Rev. 120 (2017) 25–40.
- [92] M. Rigato, M. Monami, G.P. Fadini, Autologous cell therapy for peripheral arterial disease: systematic review and meta-analysis of randomized, nonrandomized noncontrolled studies, Circ. Res. 120 (8) (2017) 1326–1340.
- [93] H.M. Wobma, D. Liu, G. Vunjak-Novakovic, Paracrine effects of mesenchymal stromal cells cultured in three-dimensional settings on tissue repair, ACS Biomater. Sci. Eng. 4 (4) (2018) 1162–1175.